ORIGINAL ARTICLE

Synthesis and in silico evaluation of 1*N*-methyl-1*S*-methyl-2-nitroethylene (NMSM) derivatives against Alzheimer disease: to understand their interacting mechanism with acetylcholinesterase

**M. Kannan · P. Manivel · K. Geetha ·
J. Muthukumaran · H. Surya Prakash Rao · R. Krishna**

Abstract Anomalous action of human acetylcholinesterase (hAChE) in Alzheimer's disease (AD) was restrained by various AChE inhibitors, of which the specific and potent lead candidate Donepezil is used for treating the disease AD. Besides the specificity, the observed undesirable side effects caused by Donepezil invoked the quest for new lead molecules with the increased potency and specificity for AChE. The present study elucidates the potency of six 1*N*-methyl-1*S*-methyl-2-nitroethylene (NMSM) derivatives to form a specific interaction with the peripheral anionic site and catalytic anionic subsite residues of hAChE. The NMSMs were prepared in good yield from 1,1-di(methylsulfanyl)-2-nitroethylene and primary amine (or) amino acid esters. In silico interaction analysis reveals specific and potent interactions between hAChE and selected ligand molecules. The site-specific interactions formed between these molecules also results in a conformational change in the orientation of active site residues of hAChE, which prevents them from being accessed by beta-amyloid protein (Aβ), which is a causative agent for amyloid plaque formation and acetylcholine (ACh). In silico interaction analysis between the ligand-bounded hAChE with Aβ and ACh confirms this observation. The variation in the conformation of hAChE associated with the decreased ability of Aβ and ACh to access the respective functional residues of hAChE induced by the novel NMSMs favors their selection for in vivo analysis to present themselves as new members of hAChE inhibitors.

Introduction

Alzheimer's disease is the most progressive and fatal brain disease, which attributes to the loss of memory and influences the learning process in the affected individuals. Alzheimer's disease (AD) affected individuals were characterized by the presence of senile plaques and neurofibrillary tangles in their brains [1, 2]. Loss of memory is directly correlated with the abridged cholinergic neuro-transmission, caused by the pronounced diminish in the levels of the neurotransmitter, ACh. Abnormal activity of human acetylcholinesterase (hAChE), the enzyme responsible for hydrolysis of ACh, was attributed to the reduced level of ACh. Treating AD was achieved through inhibiting the anomalous action of AChE [3–6] by various specific AChE inhibitors [7] such as Donepezil (Aricept®) [8], Tacrine (COGNEX®) [9], and Rivastigmine (EXELON®) [10].

The catalytic triad (CT) formed by the residues Glu334, His447, and Ser203 [11], placed at about 4 Å from the base of the gorge, has a direct consequence on the hydrolysis of ACh. CT is placed at the end of the aromatic gorge composed of 11 aromatic amino acids, which span half way into the enzyme [12, 13]. Nucleophilic attack of the substrate carbonyl carbon by the Ser203 hydroxyl generates an intermediate acyl-enzyme and choline molecule. This intermediate molecule is released through the active participation of His447-NE2 with Ser203-OG and His447-ND1 with

M. Kannan · P. Manivel · J. Muthukumaran · R. Krishna (✉)
Centre for Bioinformatics, Pondicherry University,
Pondicherry 605 014, India
e-mail: krishstrucbio@gmail.com

K. Geetha · H. S. P. Rao (✉)
Department of Chemistry, Pondicherry University,
Pondicherry 605 014, India
e-mail: hspr@yahoo.com

H. S. P. Rao
e-mail: hspr.che@pondiuni.edu.in

Glu334-OE1 by the corresponding hydrogen bond distances of about 2.8 and 2.6 Å, respectively [14]. Most of the administered drugs interact with the CT of AChE [15, 16]. Furthermore, their interaction with residues (Trp86 and Tyr337) of catalytic anionic subsite (CAS), placed in close proximity to the active site, influences the hydrolysis of ACh [9, 13, 17–19]. Besides the CT and CAS, the residues of peripheral anionic site (PAS; Tyr72, Asp74, Tyr124, Trp286, and Tyr341) also influence the function of AChE through their allosteric effects [16, 20, 21]. Residues of PAS trap the substrate molecules as they enter the gorge, and are involved in accelerating the transfer of the substrate acyl group to a serine hydroxyl group in CAS [17, 18, 22–25]. In addition, PAS site is potentially responsible for colocalization of amyloid-β (Aβ) peptide in the brains of AD patients and has been shown to accelerate the assembly of Aβ to form amyloid fibrils [26–28].

Several ligands capable of binding at PAS site of hAChE have been shown to retard aggregation of Aβ [28, 29]. Besides interacting with residues of CT, drugs aimed at interaction with this site were found to bind with human butylcholinesterase (hBChE), a homologue of hAChE [30, 31]. This unspecific interaction results in many undesired effects such as nausea, vomiting, loss of appetite, increased frequency of bowel movements, and possible liver damage [32–35]. The close structural analysis of these two homologues reveals the absence of PAS site in hBChE. This observation leads to the design of specific inhibitors, which can interact precisely with the residues of PAS and CAS in the gorge can act as the potent inhibitors of hAChE allosterically.

Donepezil, a cholinesterase inhibitor, is one such drug candidate with high specificity for AChE [36] and was designed to interact exclusively with CAS (π–π stacking with Trp86; cation–π interaction with Phe330) and PAS (Tyr124) site residues [8]. Besides the strong interacting abilities of Donepezil, its administration as drug was also associated with several undesirable effects [37, 38]. The observed undesirable effects associated with administration of various hAChE inhibitors initiated the quest for the design of specific and potent hAChE inhibitors, which can precisely interact with residues of PAS and also can span the gorge so as Donepezil.

Accordingly, in the present study, the effectiveness of the NMSM derivatives was evaluated to inhibit the action of hAChE through in silico studies. NMSM is the starting compound in the manufacture of antiulcer drug Ranitidine [39, 40]. Initially, the library of NMSM derivatives was screened based on their absorption, distribution, metabolism, excretion, and toxicity (ADMET) and Lipinski's rule of five, which resulted in 12 compounds as the best hits. All the 12 compounds were subjected into TarFisDock [41, 42] server to find out their protein target. A result of such analysis for the given compounds suggested that they might have an ability to interact with hAChE. The interacting

ability of these compounds was analyzed in detail concerning the interaction mechanism of Donepezil. Later, the compounds (six), which exhibited specific interactions with both CAS and PAS site residues of hAChE, were selected. Finally, the ability of the ligand-bounded conformations to block the interaction of hAChE with Aβ and ACh was analyzed. The selected compounds were found to have similar interacting features so as Donepezil by making interactions with both CAS and PAS site residues of hAChE, which suggests the possibility for the selection of these compounds to evaluate their efficacy and to act as the new class hAChE inhibitors, through various in vivo and in vitro approaches.

Materials and methods

Lead screening and toxicity prediction analysis

The library of compounds that belongs to NMSM derivatives was analyzed for their biological activities. The synthesis of the NMSM derivatives are given in "Experimental section." The structure of the compounds was drawn using Marvin Been software v 5.1.1(http://www.chemaxon.com/marvin/). The three-dimensional structures were prepared by prepare ligand module in Accelrys discovery studio (DS) suite (Version 2.1, Accelrys Software Inc.). These compounds were then subjected to the analysis of ADMET properties using ADMET module of DS. From the obtained results, 12 of the total compounds that satisfied all the ADMET properties were selected and checked for the possible side effects and toxicity using Osiris Property Explorer (http://www.organic-chemistry.org/prog/peo/) and PASS software [43, 44]. The pharmacological properties of these compounds as desired for a drug molecule were predicted by Molinspiration (http://www.molinspiration.com/cgi-bin/properties). Toxicity prediction (TOPKAT) protocol of DS was also used to predict the toxic nature of the compound with available toxic compounds in the database using quantitative structure toxicity relationship models. Finally, the drug-like score was also computed for the selected ligands by PASS Program.

Molecular Docking

The prepared compounds were subjected to TarFisDock server for identifying the biological target, the result of which shows that all the six ligands might act as good inhibitors for the hAChE. In order to confirm the interacting capability of these compounds towards hAChE, the manual docking analysis was carried out using the Genetic Optimization for Ligand Docking (GOLD) V4.0.1 [45, 46] docking suite, which employs a genetic algorithm to find the different ligand binding modes. The crystal structure of hAChE

(PDB ID: 1B41) [47] was chosen for docking analysis. Water molecules were removed, and hydrogen atoms were added to the protein molecule prior to the docking procedures. The active site intended for docking was defined using the coordinate information of the residue Tyr72 of hAChE. Binding site radius was given as 10 Å, and population size was set to 100. Selection pressure was set to 1.1; niche size was set to 2, and the number of populations to be performed is set to 100,000. GOLD scoring function was used to score the best interacting ligands. Generally, the higher the value, the higher is the binding affinity of the ligands. The ligands that exhibit more efficient interacting ability in terms of docking score, type of interactions, and residues interacted so as that of Donepezil were selected and their interacting mechanism with the residues of PAS and CAS was analyzed. The prediction of pKa values of protein–ligand complexes are of great practical importance to rational drug design because the strength of ligand binding (i.e., the binding free energy) is dependent on the protonation states of the ionizable residues and functional groups in the active site. Hence, the pKa calculations of protein–ligand complex are calculated using PROPKA 2.0 Web Interface online server, and the results were analyzed [48].

Docking studies of AChE with its agonists (ACh and Aβ)

Docking studies were carried out between the selected hAChE–ligand complex with Aβ (PDB ID: 1HZ3) [49] and ACh to evaluate their ability to inhibit the interactions between AChE and their agonists, respectively. Previously, to gain the information of native hAChE (ligand free protein PDB ID: 1B41) interaction with their agonists, a separate docking study between native hAChE and their agonists was also performed. GOLD suite V4.0.1 with the docking parameter mentioned above was used for performing the interaction analysis of ACh with native hAChE and hAChE–ligand-bounded complex, respectively. Interaction studies were carried out using the coordinate information of the residue Ser203-OG of hAChE. HADDOCK web server [50] was then used for understanding the interaction between Aβ with native hAChE and ligand-bounded conformation of hAChE. For doing this, the PAS site of hAChE and active site of Aβ were defined using the residues Try72, Asp74, Pro78, Tyr124, Trp286, Tyr337, Tyr341, Gly342 and Val18, Phe19, Phe20, Val24, Gly25, Gly29, Gly33, respectively.

Results and discussion

Synthesis of NMSM derivatives

The selected three primary amines and three essential amino acid methyl esters were reacted in a single-pot operation, with

the nitroketene S,S-acetal (1,1-di(methylsulfanyl)-2-nitroethylene) [51, 52] in acetonitrile reflux to furnish corresponding nitroketene N, S-acetals (Lig_1, 2, 3, 4, 5, and 6) in good yields (Schemes 1 and 2). The yields of the product and reaction time for synthesis of nitroketene N,S-acetals and the amino acid containing nitroketene N,S-acetals are given in Table 1.

### Prediction of drug likeness and toxicity for the selected compounds

The results of ADMET, Lipinski's, and docking score with hAChE screening procedures reveals that 6 of 12 NMSM derivatives compounds are nonhepatotoxic and noninhibitors of cytochrome P450 enzymes. These compounds were also found to have more efficiency to cross the blood–brain barrier with good absorption and high solubility nature. Osiris Property Explorer and TOPKAT predicted results confirm that these compounds were not associated with any toxicity risks. PASS software evaluation ($P_a > P_i$) predicted that there are no possible side effects and their drug likeliness was also disclosed by the predicted drug-like scores. The topological polar surface area (TPSA) [53], number of ON group (n_{ON}), number of OHNH group (n_{OHNH}) and number of violation ($n_{Violation}$—all values are zero) predicted by Molinspiration analysis favor their drug-like nature (Table 2). The **Lig_1** (ID: 9725121), **Lig_3** (ID: 10377907), and **Lig_4** (ID: 10377911) are already available in ChemSpider database and are shown to be with anti-AChE activity, which is confirmed through their SIM-BIOSYS LASSO score (http://www.chemspider.com). The remaining **Lig_2**, **Lig_5**, and **Lig_6** are novel compounds shown to be one of the derivatives of Ranitidine [54] and abovementioned group. The two-dimensional structures of all compounds are shown in Fig. 1, and synthesis of these six ligands is given in "Experimental section."

Molecular docking

To study the molecular basis for interacting mechanism and affinity of NMSM derivatives with hAChE, all these ligands were docked in PAS site of hAChE. The docking result of these ligands in comparison with Donepezil was analyzed, and the hydrogen bond, van der Waals interaction residues, GOLD score, external H bond (HB) and external van der Waals (VdW) scores are listed in Table 3. The GOLD score determines the fitness of the ligands in PAS and CAS site of hAChE, and the external HB and VdW scores represent the hydrophobicity and hydrogen-bonding capacity of the ligands towards the hAChE in the same site.

Docking of Donepezil with hAChE

Donepezil is a potent inhibitor of tAChE, and it has a full gorge spanning capacity towards tAChE. Hence, discussing

Scheme 1 General synthesis of nitroketene *N,S*-acetals
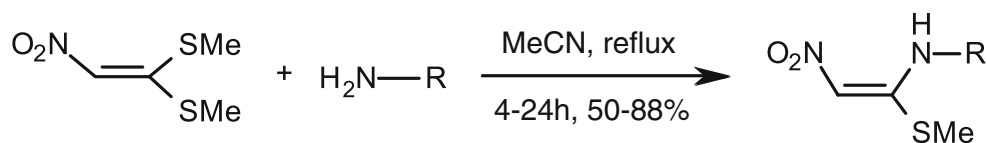
Lig_1: R = CH$_2$C$_6$H$_5$; **Lig_2**: R = (CH$_2$)$_2$C$_6$H$_5$; **Lig_3**: R = CH(CH$_3$)C$_6$H$_5$.

the binding modes of Donepezil with tAChE would boost in claiming docking results of NMSM and its derivatives with hAChE. In examining the position and orientation of the Donepezil in hAChE-PAS site predicted by our docking procedure, it was observed that side-chain hydroxyl group of Tyr337 acts as a hydrogen bond (HB) donor to make an hydrogen bond with oxygen atom of Donepezil with maximum bond length of 2.67 Å (Fig. 2a). The PAS, CAS, oxyanion hole (Gly120 and Gly121), CT, acyl binding pocket (Phe297 and Phe338), and other residues Leu76, Trp117, Tyr119, Leu130, Ser293, Val294, Arg296, and Ile451 of hAChE were involved in van der Waals (VdW) contacts. In close assessment of this binding mode, the Trp86 and Trp286 were found to make overlap of two adjacent site stacked [55] interactions with benzyl ring and dimethoxyindanone ring, respectively, instead of making π–π stacked interaction as compared with crystal structure of Donepezil–tAChE complex [8]. The GOLD score, external H bond (E-HB) and external van der Waals (E-VdW) scores for Donepezil were 51.2624, 0.3207, and 45.4531, respectively. The docking studies of Donepezil with hAChE showed that the interaction were in good agreement with experimentally determined Donepezil–tAChE complex. The clear enumeration of Donepezil-binding mode with hAChE is given in Fig. 2b.

Docking of Lig_1 to PAS of hAChE

The docked complex of **Lig_1**–hAChE shows that this ligand is orienting perpendicular to the PAS and CAS site of the gorge and positioned by the active participation of hydrogen bonds, VdW contacts and C–H–π interactions (Table 3). The N3 (P_{pKa}=7.78) of this ligand ideally positioned for a hydrogen bonding with OG group of Ser125 with distance of 3.08 Å. The nitro group establishes three HBs, in which O5 forms two HBs with OH of Tyr124 (P_{pKa}=18.40) (2.88 Å), and Tyr337 (P_{pKa}=18.25)

(2.97 Å), which is a mediator residue for the mid-point of the diameter gorge [17] and responsible for the regulation of substrate and product trafficking. Atom O6 of the nitro group forms a hydrogen bond with Tyr124 with a distance of 2.75 Å. The four hydrogen bonds formed between **Lig_1**, and hAChEs were also satisfying the PROPKA calculation (Table 4). The amino acid residues in PAS (Tyr72, Asp74, and Tyr124), CAS (Trp86 and Tyr337), oxyanion hole (Gly121), and other residues (Val73, Asn87, Pro88, and Ser125) were involved in VdW interaction with **Lig_1** (Table 3) facilitating for their active trap through entrance, base, and oxyanion hole to reach the middle of the gorge, respectively. Of these, Pro88 was found to be targeted by fasciculin [28], a peptide inhibiting the Aβ binding, ensuring that the observed interaction might hinder the binding of Aβ. The methylsulfanyl group faces the six-membered ring of the Trp86 indole by the active C–H–π interaction with a distance of 3.23 Å, which is similar to cation–π interaction as observed in the ACh–hAChE complex. The benzyl group of this ligand forms two adjacent site-stacked interaction with Tyr124 by the distance of 4.09 Å (Tyr124 CZ-C12 **Lig_1**) and 3.87 Å (Tyr124 CE1-C13 **Lig_1**), which is crucial residues of PAS site and helping for substrate binding and trafficking [17]. These results reveal that this ligand can span the entire gorge of hAChE, which might attribute to the inhibition of Aβ deposition and to the reduction in the hydrolysis of ACh (Fig. 3a).

*Docking of Lig_2 to PAS of hAChE*

The interacting conformation of **Lig_2** with hAChE reveals the presence of HBs with Asp74 (P_{pKa}=4.13), Trp86, Tyr124 (P_{pKa}=14.73), Ser125, Tyr337 (P_{pKa}=16.65), and Tyr341 (P_{pKa}=21.13), and VdW interaction with Tyr72, Asp74, Asn87, Gly121, Ser125, Tyr337, and Trp86 of CAS and PAS. The N3 (P_{pKa}=8.48) group of this ligand positioned towards Ser125 OG as **Lig_1**–hAChE complex
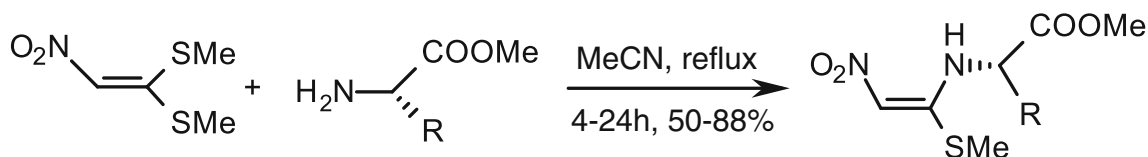

Lig_4: R = CH$_2$C$_6$H$_5$; **Lig_5**: R = CH(CH$_3$)CH$_2$CH$_3$; **Lig_6**: R =CH$_2$(C$_8$H$_6$N).

Scheme 2 General synthesis of amino acid containing nitroketene *N,S*-acetals

Table 1 Synthesis of nitroketene N,S-acetal and amino acid substituted nitroketene N,S-acetal from S,S-acetal reaction with primary amines and amino acid esters

Entry	Primary amine and amino esters	Product nitroketene N,S-acetal	Time (h)	Yield (%)
1	$H_2N–CH_2C_6H_5$	O_2N N(H)–$CH_2C_6H_5$ / SMe **Lig_1**	9	84
2	$H_2N–(CH_2)_2C_6H_5$	O_2N N(H)–$(CH_2)_2C_6H_5$ / SMe **Lig_2**	3	72
3	$H_2N–CH(CH_3)C_6H_5$	O_2N N(H)–$CH(CH_3)C_6H_5$ / SMe **Lig_3**	5	50
4	H_2N– COOMe / CH_2Ph	O_2N N(H) COOMe / CH_2Ph / SMe **Lig_4**	24	57
5	H_2N– COOMe / $CH(CH_3)CH_2CH_3$	O_2N N(H) COOMe / $CH(CH_3)CH_2CH_3$ / SMe **Lig_5**	18	53
6	H_2N– COOMe / $CH_2(C_8H_6N)$	O_2N N(H) COOMe / $CH_2(C_8H_6N)$ / SMe **Lig_6**	17	48
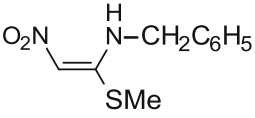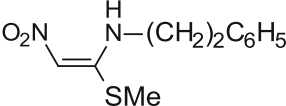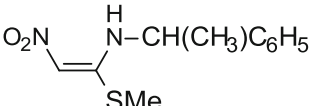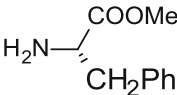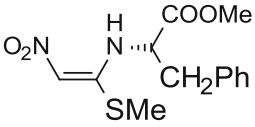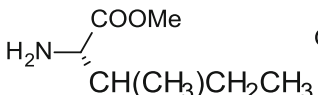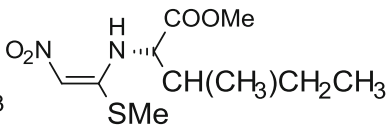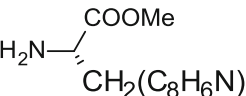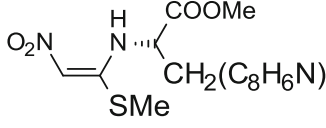
The reaction time and product yields are also described for each compound

with the HB distance of 2.79 Å. The nitro group of O5 make HBs with Tyr337 OH (2.08 Å), Tyr341 OH (2.63 Å), and Asp74 OD1 (2.70 Å), respectively, whereas the O6 atom forms HB with Tyr124 OH (2.87 Å) and Asp74 OD1 (2.79 Å), which are the crucial residues of PAS and CAS of hAChE. The methylsulfanyl group establishes the HB between S7 and O of Trp86 with a distance of 3.29 Å. The

benzyl ring (Cg: C11, C12, C13, C14, C15, and C16) of this ligand faces the six-membered ring of the Trp86 indole by the strong π–π stacking interaction with the distance of 3.47 Å so as observed in Donepezil–tAChE complex [8] (Fig. 3b). These results in comparison with both Donepezil and **Lig_1**, reveals that this **Lig_2** might have high priority to interact with hAChE.

Table 2 Molecular formula, Lipinski's rule of five, drug-like score, and Molinspiration analysis of selected NMSM derivatives

Leads	Molecular formula	Lipinski's rule of five and PASS analysis						Molinspiration analysis		
		Molecular weight	ALog$P$	Rotatable bonds	Acceptor	Donors	Drug-like score	TPSA	n_{ON}	n_{OHNH}
Lig_1	$C_{10}H_{12}N_2O_2S$	224.28	2.10	5	4	1	0.053	57.851	4	1
Lig_2	$C_{11}H_{14}N_2O_2S$	238.31	2.42	6	4	1	0.105	57.851	4	1
Lig_3	$C_{11}H_{14}N_2O_2S$	238.31	2.48	5	4	1	0.082	57.851	4	1
Lig_4	$C_{13}H_{16}N_2O_4S$	296.34	2.27	8	6	1	0.246	84.156	6	1
Lig_5	$C_{10}H_{18}N_2O_4S$	262.32	2.01	8	6	1	0.462	84.156	6	1
Lig_6	$C_{15}H_{17}N_3O_4S$	335.38	2.56	8	6	2	0.353	99.947	7	2

Fig. 1 The two dimensional structure of six selected NMSM derivatives with its corresponding IUPAC names used in this study
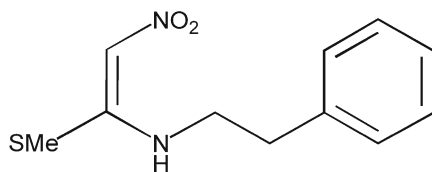
Lig_1: N-Benzyl-N-[(E)-1-(methylsulfanyl)-2-nitro-1-ethenyl] amine
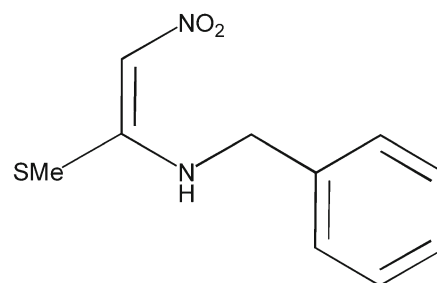
Lig_2: N-[(E)-1-(Methylsulfanyl)-2-nitro-1-ethenyl]-N-phenethylamine
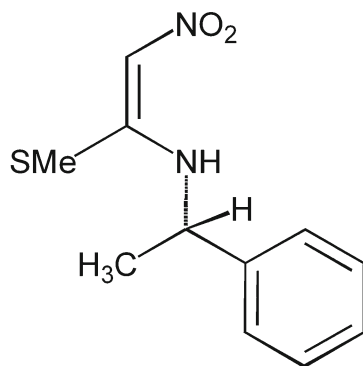
Lig_3: N-[(E)-1-(methylsulfanyl)-2-nitro-1-ethenyl]-N-[(1S)-1-phenylethyl]amine
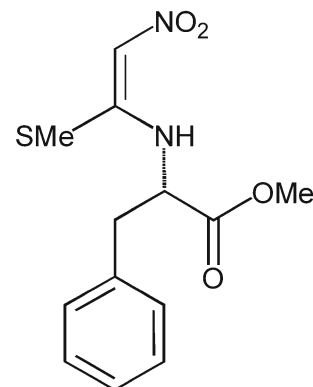
Lig_4: Methyl (2S)-2-[(E)-1-(methylsulfanyl)-2-nitro-1-ethenyl]amino-3-phenylpropanoate
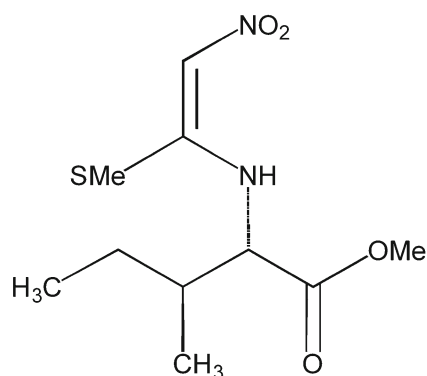
**Lig_5:** Methyl (2S,3S)-3-methyl-2-[(E)-1-(methylsulfanyl)-2-nitro-1-ethenyl]aminopentanoate
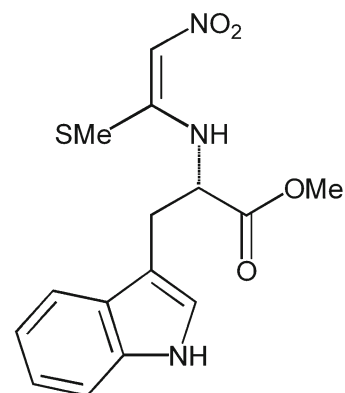
Lig_6: Methyl (2S)-3-(1H-3-indolyl)-2-[(E)-1-(methylsulfanyl)-2-nitro-1-ethenyl]aminopropanoate

Table 3 Molecular interactions of hAChE with selected NMSM derivatives

Name	Hydrogen bond interaction			VdW interaction residues	GOLD score	E-HB score	E-VdW score
	H bond donor	H bond acceptor	H bond length (Å)				
Lig_1	Lig:: N3	Ser125: OG	3.08	Tyr72, Val73, Asp74, Trp86, Asn87, Pro88, Gly121, Tyr124, Ser125	48.8759	12.3196	29.0771
	Tyr124: OH	Lig:: O5	2.88				
	Tyr337: OH	Lig:: O5	2.97				
	Tyr124: OH	Lig:: O6	2.75				
Lig_2	Lig:: N3	Ser125: OG	2.79	Tyr72, Asp74, Trp86, Asn87, Gly121, Tyr124, Ser125, Tyr337	58.4975	14.0000	34.5834
	Tyr337: OH	Lig:: O5	2.08				
	Tyr341: OH	Lig:: O5	2.63				
	Asp74: OD1	Lig:: O5	2.70				
	Asp74: OD1	Lig:: O6	2.79				
	Tyr124: OH	Lig:: O6	2.87				
	Trp86: O	Lig:: S7	3.29				
Lig_3	Lig:: N3	Ser125: OG	2.95	Tyr72, Val73, Asp74, Trp86, Asn87, Pro88, Gly121, Tyr124, Ser125, Tyr337	51.3776	13.0085	31.9722
	Tyr124: OH	Lig:: O5	2.79				
	Tyr124: OH	Lig:: O6	2.87				
	Tyr337: OH	Lig:: O6	2.73				
Lig_4	Trp86: NE1	Lig:: O12	2.72	Asp74, Thr83, Trp86, Gly121, Tyr124, Ser125, Glu202, Ser203, Tyr337	55.3405	3.1110	43.6953
	Lig:: O5	Trp86: O	3.02				
	Lig:: O6	Gly121: O	2.62				
Lig_5	Ser125: OG	Lig:: O12	2.76	Asp74, Trp86, Asn87, Gly122, Ser125, Ser203, Phe297, Tyr337, Phe338	50.3519	14.9506	33.0904
	Lig:: N3	Tyr337: OH	2.83				
	Tyr124: OH	Lig:: O5	2.82				
	Tyr337: OH	Lig:: O6	2.95				
Lig_6	Lig:: N3	Ser125: OG	2.60	Tyr72, Asp74, Trp86, Asn87, Gly120, Gly121, Tyr124, Glu202, Phe297, Tyr337, Tyr341	71.7483	15.3282	46.8844
	Lig:: S7	Trp86: O	3.21				
	Tyr124: OH	Lig:: O6	3.21				
	Tyr341: OH	Lig:: O6	3.04				
	Asp74: OD2	Lig:: O6	3.21				
	Tyr337: OH	Lig:: O6	2.29				
	Tyr124: OH	Lig:: O5	2.43				
	Tyr124: OH	Lig:: O13	2.96				
	Tyr337: OH	Lig:: O12	2.45				
Donepezil	Tyr341: OH	Lig:: O23	3.08	Tyr68, Trp82, Gly116, Gly117, Tyr120, Gly122, Leu126, Tyr129, Trp276, Phe287, Tyr327, Phe328	51.2624	0.3207	45.4531

Docking of Lig_3 to PAS of hAChE

The interaction of **Lig_3** with hAChE was stabilized through the formation of HBs, VdW, and C–H–π interactions. The nitro group of **Lig_3** makes three tight HBs with Tyr124 (P_{pKa}=16.58) and Tyr337 (P_{pKa}=20.16), in which Tyr124 OH group makes two HBs with O5 and O6 of **Lig_3** with a distance of 2.79 Å and 2.89 Å, respectively, and the remaining was formed between Tyr337 OH and O6 of **Lig_3** by a contact distance of 2.73 Å. Moreover, the N3 (P_{pKa}=7.76) atom of this ligand is placed towards the conserved Ser125 so as in **Lig_1** and **Lig_2**–hAChE complexes with bond distance of

about 2.95 Å. This ligand also makes VdW interactions with the residues of PAS site (Tyr72, Asp74, and Tyr124), CAS site (Trp86 and Tyr337), oxyanion hole (Gly121) [56], and with other residues (Val 73, Asn87, Pro88, and Ser125) of hAChE. The C–H–π interaction was formed by the position of **Lig_3** methylsulfanyl group towards the benzyl ring of Trp86 indole with a distance of 2.79 Å, which is mainly focused for their contribution in the gorge, similar to cation–π interaction of ACh–hAChE complex. Although the obtained GOLD score for the interactions made by this ligand is 51.3776, which are lesser than **Lig_2**–hAChE interaction, yet strong hydrophobic, C–H–π, and HB interactions with residues of both PAS
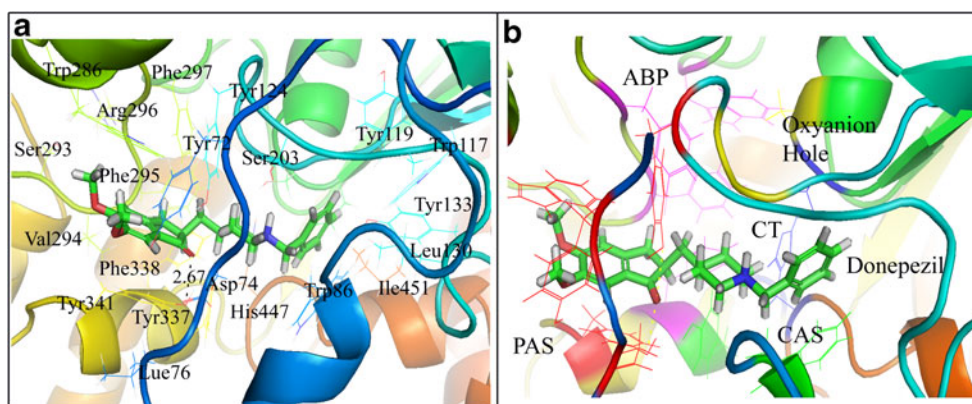
Fig. 2 The molecular interaction of Donepezil with hAChE complex. **a** Hydrogen bond and VdW contacts formed between Donepezil and hAChE. **b** Donepezil binds along the CT region and interacts with the PAS site at the top. This also makes interaction with oxyanion hole at the middle and binds with acyl binding pocket (ABP) [color codes: *red line* representation is PAS site; *green line* is CAS; *blue line* is CT region; and *magenta line* is acyl binding pocket (ABP)]

and CAS site make this ligand a more promising compound for in vitro analysis so as other compounds (Fig. 3c).

Docking of Lig_4 to PAS of hAChE

In the **Lig_4**–hAChE docked complex, ligand conformation was stabilized by HB and VdW interactions with Asp74 (P_{pKa}=3.46), Thr83, Trp86, Gly120, Gly121, Tyr124 (P_{pKa}=

13.51), Ser125, Glu202 (P_{pKa}=10.76), Ser203, and Tyr337 (P_{pKa}=20.73). Of these, Ser203, a CT residue is responsible for the hydrolysis of ACh molecule, whereas the residues of PAS, oxyanion hole, and CAS were involved in the active participation of substrate entry, trap and hydrolysis process of ACh. The present orientation of this ligand is observed to block binding of ACh; thereby, it acts as the full gorge spanning ligand. The nitro group establishes the two HBs, one with

Table 4 The predicted pKa values calculated using PROPKA 2.0 for ligand–hAChE complexes

This includes predicted pKa values, interacting atoms and type of interaction. P_{pKa} is predicted pKa, pKamodel for Tyr is 10, Asp is 3.80, Glu is 4.50, and ligand N3 is 10.

Protein-ligand complex	Active site Residue and ligands	P_{pKa}	Interacting Residues and atoms of Ligand	Interaction type
hAChE-Lig_1	Tyr124	18.40	UNK: O5 & O6	HB & VdW
	Tyr337	18.25	UNK:O5	
	UNK: N3	7.78	Ser125:: OG	
hAChE-Lig_2	Asp74	4.13	UNK: O5 & O6	HB & VdW
	Tyr124	14.73	UNK: O6	
	Tyr337	16.65	UNK: O5	
	Tyr341	21.13	UNK: O5	
	UNK: N3	8.48	Ser125:: OG	
hAChE-Lig_3	Tyr124	16.58	UNK: O5 & O6	HB & VdW
	Tyr337	20.16	UNK: O6	
	UNK: N3	7.76	Ser125:: OG	
hAChE-Lig_4	Asp74	3.46	Lig_4	VdW
	Tyr124	10.76		
	Glu202	13.51		
	Tyr327	20.73		
	UNK: N3	6.49		
hAChE-Lig_5	Tyr124	17.19	UNK: O5	HB & VdW
	Tyr327	21.89	UNK: O6	
	UNK: N3	6.96	Tyr337: OH	
hAChE-Lig_6	Asp74	3.90	UNK: O6	HB & VdW
	Tyr124	21.16	UNK: O6, O5 & O13	
	Tyr337	15.46	UNK: O6 & O12	
	Tyr341	19.80	UNK: O6	
	UNK: N3	8.09	Ser125:: OG	

Fig. 3 The molecular interaction of PAS and CAS site of hAChE with six of selected NMSM derivatives based on comparison with Donepezil docking score and interacting residues: **a** Lig_1–hAChE complex, **b** Lig_2–hAChE complex, **c** Lig_3–hAChE complex, **d** Lig_4–hAChE complex, **e** Lig_5–hAChE complex, and **f** Lig_6–hAChE complex. The interactions are shown in *dashed lines* [color codes: *green* HBs, *blue* C–H–π and π–π stacking interactions; *Cg* represents the centroid of five or six membered ring]
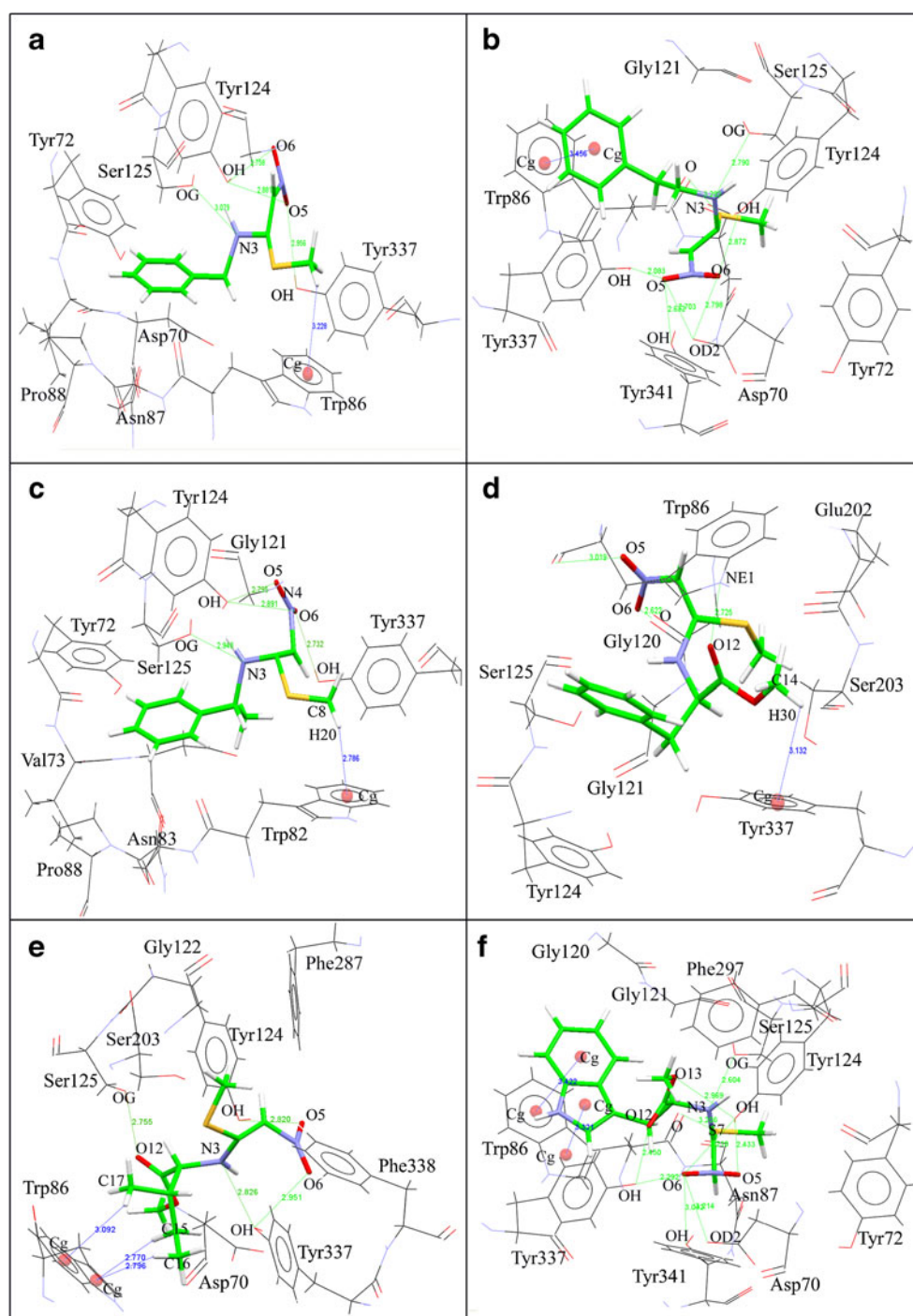
O6 and Gly121 O and another with O5 and Trp86 O by the contact distance of 2.62 and 3.02 Å, respectively. The O12 atom of **Lig_4** faces the five-membered ring of Trp86 and forms an HB with NE1 (2.72 Å). The O12 atom also makes a strong VdW contact with indole ring (CD1, CG, and CD2) of Trp86 by the distance of 2.64, 2.56, and 2.64 Å, respectively. Amidst all the observed interactions, the *O*-methyl group positioned towards the phenyl group of Tyr337 by the strong C–H–π interaction with a short contact distance of 3.13 Å. All these interactions mark a potential effect induced on the

structure of hAChE, which provokes the possible inhibitory effect on the deposition of Aβ and on the reduction of ACh hydrolysis by hAChE (Fig. 3d).

Docking of Lig_5 to PAS of hAChE

In the assessment of position and orientation of **Lig_5**–hAChE docked complex, the side-chain hydroxyl group of Tyr337 (P_{pKa}=21.89) makes two hydrogen bonds with N3 and O6 atom of **Lig_5** with a distance of 2.83 and 2.95 Å,

respectively. The OH group of Tyr124 (P_{pKa}=17.19) and OG of Ser125 were found to form HBs with O5 and O12 atom of **Lig_5** with a distance of 2.82 and 2.76 Å, respectively. In addition, the binding interactions are dominated by VdW contacts observed in the residues of Asp74 (P_{pKa}= 3.06), Trp86, Asn87, Gly122, Ser125, Ser203, Phe297, Tyr337, and Phe338 (acyl pocket residue). As **Lig_1**, this ligand also lacks the cation–π and π–π interaction, but it forms the stable C–H…π interaction between C16–H30, C15–H27 with five membered ring (Cg: CD1, CG, CD2, NE1, and CE2) and C17–H32 with benzyl ring (Cg: CD2, CE2, CZ2, CH2, CZ3, and CE3) of Trp86 in a distance of 2.79, 2.77, and 3.10 Å, respectively (Fig. 3e). The GOLD, E-HB, and E-VdW scores for this ligand were 50.3619, 14.9506, and 33.0904, respectively. The obtained results indicate that this ligand might have a similar effect as **Lig_1**, **Lig_3**, and **Lig_4** and a lesser effect than **Lig_2**.

Docking of Lig_6 to PAS of hAChE

In comparison of interaction results of Lig_6–hAChE complex with aforementioned ligand–hAChE complexes, Lig_6 shows efficient interactions with hAChE (Table 3) and oriented perpendicular to the PAS and CAS site of the gorge by the active HBs, VdW, and π–π stacking interactions. The nitro groups of this ligand form five HBs, in which O6 atoms make four HBs with Tyr124 OH (3.21 Å), Tyr341 OH (3.04 Å), Asp74 OD2 (3.21 Å), and Tyr337 OH (2.29 Å); whereas O5 forms a HB with Tyr124 OH (2.43 Å). The *O*-methoxy group of **Lig_6** forms a hydrogen bond with Tyr124 OH (2.96 Å) and O12 atom positioned to Tyr337 OH with a distance of 2.45 Å. The N3 (P_{pKa}=8.09) atom is directed towards Ser125 OG by the HB distances of 2.60 Å as like **Lig_1**, **Lig_2**, and **Lig_3**. The methylsulfanyl group positioned towards the backbone oxygen atom of Trp86 and forms an HB bond by the distance of 3.21 Å (Fig. 3f). The conserved amino acid residues of PAS and CAS [Tyr72, Asp74 (P_{pKa}=3.09), Trp86, Asn87, Gly120, Gly121, Tyr124 (P_{pKa}=21.16), Tyr337 (P_{pKa}=15.46), and Tyr341 (P_{pKa}=19.80)], and the nonconserved residues Gly122, Glu202, and Phe296 were also involved in making VdW contact with ligand by the GOLD score of 71.7483, E-HB score of 15.3282, and E-VdW score of 46.8844. In addition to the observed interactions, a strong π–π stacking interaction is formed with indole ring of Trp86, which marks this ligand as the potential drug candidate than the other ligands of this group. These π–π stacking interactions were made between the indole ring of **Lig_6** (Cg1: C15, C16, C17, C18, C21, and C22;, Cg2: C19, C20, C21, C22, and N23) and indole ring of Trp86 (Cg3: benzyl ring of Trp86; Cg4: pyrrole ring of Trp86) with a distance of 3.422 (Cg1–Cg3) and 3.321 (Cg2–Cg4)Å, respectively.

**Docking studies of hAChE with its agonists (ACh and Aβ)**

Interaction of hAChE–ACh and Lig_6hAChE–ACh complexes

The docking of native hAChE–ACh complex elucidates the HBs between Ser203 OG and C5 and O4 of ACh with a distance of 2.63 and 2.81 Å, respectively. Considerably, another HB with a distance of 2.87 Å was observed with NE2 of His447, which is a catalytic partner of Ser203, and this interaction is responsible for the proton transfer and thereby favors the catalytic mechanism of hAChE. Two more hydrogen bond also formed between Gly122-N and O7 and His447-NE2 and O4 of ACh with distance of 2.72 and 3.17 Å, respectively (Fig. 4a). The N1 of ACh makes the cation–π interaction with Trp86 by the distance of 4.17 Å (Table 5). The residues of Trp86, Gly122, Ser203, Phe295, Phe297, and His447 are actively participating in VdW contacts, which are involved in substrate trafficking of ACh to the catalytic site. All these interactions and distance values are in good agreement with that of reported crystal structure of ACh/mAChE (mouse AChE) complex [17]. However, in **Lig_6**–bound hAChE–ACh complex, the substrate molecule is positioned in PAS site instead of binding with CT region of hAChE due to the active participation of **Lig_6** in both PAS and CAS site with the GOLD score of 34.163. The acetoxy moiety of ACh located near the constricted region of the gorge interacts via oxygen with Tyr124 (2.99 Å) on one side and also via methyl group with Tyr337 on the other side (Fig. 4b). This orientation of the substrate molecules in PAS site resulted in the trafficking of ACh into the CT region by active participation of oxyanion hole residues, whereas in this case, the substrate is bound at PAS site as described by Bourne et al. in mAChE [17], but it will not move further to the CT region because of active participation of **Lig_6** in both the PAS and CAS site. As described by Bourne, the PAS-bound substrate may also limit the substrate entry to CT region, when the inhibition of catalysis by excess substrate occurs. Thus, overall, the PAS-bound conformation of ACh is mimicking the nature of the ACh binding in PAS site and thereby inhibiting the function of hAChE.

Native hAChE–Aβ and Lig_6-bound hAChE–Aβ interactions

The interaction studies of native hAChE–Aβ complex shows that residue Tyr72, Val73, Asp74, Thr75, Tyr124, Asn283, Glu295, and Trp286 of hAChE involved in making HBs with Tyr1, Glu2, His4, His5, Gln7, and Lys7 of Aβ with the HADDOCK score of −74.80. The residues Tyr72, Thr75, Lue76, Pro78, Asn283, and Trp286 of hAChE were also actively participating in VdW contacts with Tyr1, His4, Gln6, Lys7, Phe10, and Phe11 of Aβ (Table 5). These results suggested that hAChE promotes the Aβ binding in

Fig. 4 The molecular
interaction of ACh and Aβ with
native hAChE and Lig_6 bound
conformation of hAChE and
vice versa. **a** Interaction
between ACh and native
hAChE with the CT region, **b**
interaction between ACh and
Lig_6 bound hAChE; Lig_6
absorbedly kept for their
functional activity. HBs are
shown as *green dashed lines*,
VdW contacts are in *red dashed
lines*, and cation–π interaction
are in *blue dashed line*; *Cg* is
centroid of benzene ring. **c**
Interaction of Aβ with native
hAChE. **d** Molecular
interaction between Lig_6
bound hAChE with Aβ; here,
Aβ interacts with passive PAS
site, which are near the PAS site
residues. PAS site are shown in
*green colored mesh
representation*, and *violet color
mesh representation* shows the
Aβ. **e** The superimposition of
native hAChE–Aβ with Lig_6
bound hAChE–Aβ complex
shows the displacement in the
PAS binding site of hAChE, in
which *green* and *blue* are
represents the native hAChE–
Aβ complex and *magenta* and
orange indicates the Lig_6
bound hAChE–Aβ complex,
respectively
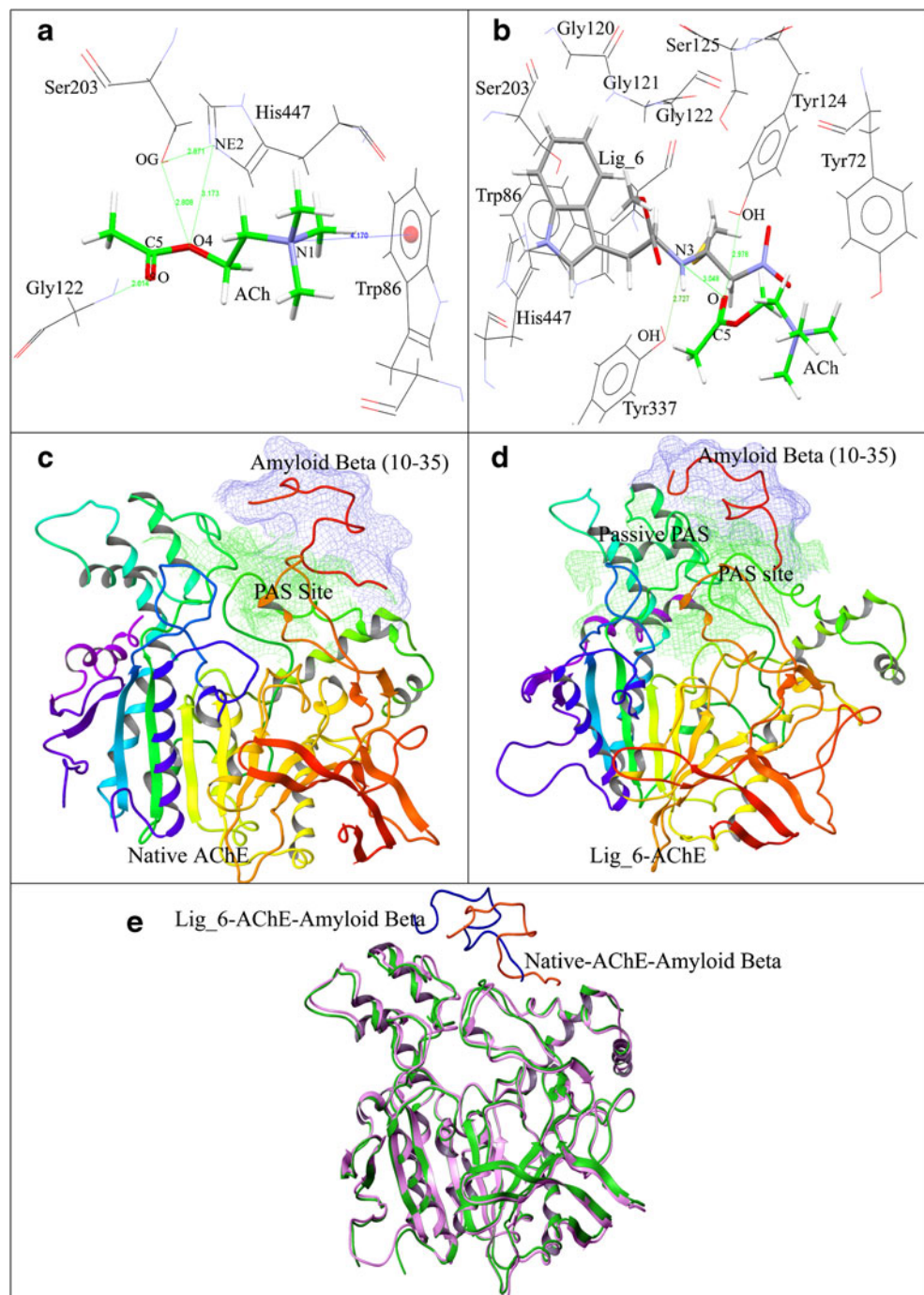
a perfect orientation through the active participation of all
PAS sites and other residues (Fig. 4c), which in turn leads to
the formation of amyloid plaque in AD patients. However,
in case of **Lig_6**-bound conformation of hAChE–Aβ
interactions, results elucidate the reduced ability of Aβ
to make strong contact with hAChE (HADDOCK score,
−28.9), which becomes evident from the absence of sev-
eral observed interactions between them as observed in
the native docking studies. In this case, besides the
involvement of Asp74, several other residues such as

Leu76, His287, Ala343, and Phe346 were also observed
to make contacts with Aβ. The deficient involvement of
Tyr72, Val73, Thr75, Tyr124, Asn283, Trp286, and
Glu285 in interaction (Fig. 4d) with Aβ depicts the alter-
ation in the conformation of hAChE induced by the bind-
ing of **Lig_6** in its PAS site (Table 5). In addition, the
observed RMSD between the native and ligand-bounded
conformation of AChE along with the displacement in the
position of Aβ in later with respect to its position in the
native complex accounts to the reduced ability of Aβ to

Table 5 Molecular interactions of native hAChE and Lig_6 bound hAChE with ACh and Aβ respectively

Interactions	HB interactions			VdW contacts	GOLD score
	HB-Donor	HB-Acceptor	HB-Distance (Å)		
Native AChE-ACh and Lig_6 bound AChE-ACh complex					
Native AChE-ACh	Ser203: OG	ACH::C5	2.63	Trp86, Gly122, Ser203, Phe295, Phe297, His447	43.7313
	Ser203: OG	ACH::O4	2.81		
	His447: NE2	ACH:: O4	3.17		
	Gly122: N	ACH:: O7	2.72		
	His447: NE2	Ser203: OG	2.87		
Lig_6 AChE-ACh	Tyr124: OH	ACH:: O7	2.99	Tyr124, Tyr337, Phe338 and Lig12	34.163
	Lig_6:: N3	ACH:: O7	2.95		
Native AChE-Aβ and Lig_6 bound conformation of AChE-Aβ interactions					
Interactions	HB interactions			VdW contacts	HADDOCK Score
	HB donor	HB acceptor	HB-Distance (Å)		
Native-AChE(A)-Aβ (B)	Tyr1(B): OH	Thr75(A): OG1	2.74	Tyr72(A):: Lys7(B)	−74.80±3.4
	His4(B): NE2	Tyr72(A): OH	2.76	Tyr72(A):: His4(B)	
	Lys7(B): NZ	Asp74(A): OD1	2.67	Thr75(A):: Phe11(B)	
	Lys7(B): NZ	Tyr124(A): OH	3.24	Thr75(A):: Tyr1(B)	
	Tyr72(A): OH	Glu2(B): OE2	2.61	Leu76(A):: Leu8(B)	
	Val73(A): N	His4(B): ND1	3.19	Leu76(A):: Phe10(B)	
	Asn283(A): ND2	His5(B): ND1	3.24	Pro78(A):: Phe11(B)	
	Glu285(A): N	Gln6(B): OE1	3.02	Asn283(A):: Gln6(B)	
	Trp286(A): N	Gln6(B): OE1	2.70	Trp286(A):: Lys7(B)	
Lig_6 bound AChE conformation (A)-Aβ (B)	Tyr1(B): N	Phe346(A): O	2.92	Tyr72(A):: Leu8(B)	−28.9±16.8
	Tyr1(B): N	Ala343(A): O	2.72	Leu76(A):: His4(B)	
	His287(A): NE2	Met26(B): SD	3.19	Leu76(A):: Tyr1(B)	
	Tyr1(B): N	Tyr77(A): OH	3.30	Tyr77(A):: Glu2(B)	
	His4(B): NE2	Leu76(A): O	2.86	Lue254(A):: Leu25(B)	
	Lys7(B): NZ	Asp74(A): OD1	2.70	Trp286(A):: Leu8(B)	
				His287(A):: Met26(B)	
				His287(A):: Phe10(B)	
				Glu291(A):: Phe11(B)	
				Glu292(A):: Phe10(B)	
				Glu292(A):: Phe11(B)	
				Ser347(A):: Glu2(B)	

make strong contacts with the residues of PAS site in the ligand-bounded conformation of hAChE (Fig. 4e). Alteration in the conformation of ligand-bounded hAChE and the observed deduction in the ability of Aβ to make strong contacts with hAChE invoke the possibility for drop in the β-amyloid fibril formation in the presence of above mentioned ligands.

Conclusions

In order to explore the inhibitory mechanism of hAChE and amyloid fibril formation, novel NMSM derivatives were synthesized for the evaluation of their ability to interact with hAChE. The in silico docking of hAChE with **Lig_1**, **Lig_2**, **Lig_3**, **Lig_4**, **Lig_5**, and **Lig_6** elucidates that they pose a

strong allosteric inhibition by forming strong HBs, VdW, C–H–π, and π–π stacking interactions in both PAS and CAS site of hAChE. Moreover, the interacting mechanism of these ligands with PAS site of hAChE directs drastic changes in the orientation of hAChE active site residues, which in turn leads to the inhibition of ACh binding. The dual inhibiting capacity of these ligands was confirmed by their activity of hindering the binding of ACh and Aβ with hAChE active site and PAS, respectively. All these results suggest that our six ligands have the strong ability to inhibit the activity of hAChE and were identified as the new members of AChE inhibitors to treat the disorders raised out of amyloid fibril formation in AD patients.

Experimental section

General

Solvents, i.e., ethanol, methanol, ethyl acetate, acetone, dichloromethane, diethyl ether, and hexanes, were distilled before use. The progression of all the reactions was monitored by thin layer chromatography plates (silica gel, 0.25 mm thickness) using hexane/ethyl acetate mixture as eluent, and the plates were visualized with iodine vapors or UV light. Column chromatography was accomplished on silica gel (100–200 mesh, Acme Synthetic Chemicals, India) using hexane-ethyl acetate as eluent. Melting points were recorded by Gallenkamp melting point apparatus and were uncorrected. The UV spectra were recorded as dilute solution in methanol using a Hitachi ratio beam U-1800 spectrometer. The IR spectra were recorded as KBr pellets using an ABB BOMEM MB 104 FT-IR spectrometer. ^{1}H-NMR (60 MHz or 400 MHz), ^{13}C-NMR (100 MHz), and DEPT-135 spectra were recorded for CDCl$_3$ solutions on a JEOL 60 MHz or Bruker-400 spectrometer with tetramethylsilane (0 ppm) or CDCl$_3$ (77 ppm) as the internal standards; J values are in Hertz. ^{1}H-NMR data are reported as follows: chemical shift [multiplicity (s=singlet, d=doublet, t=triplet, q=quartet, m=multiplet, br=broad), coupling constant, and integrations]. ^{13}C-NMR spectra were determined with ^{1}H decoupling. High-resolution mass spectra were recorded on a Water Q-TOF micro mass spectrometer using electron spray ionization mode. The amino acid esters were prepared by treating corresponding commercially available natural essential amino acids by reacting with thionyl chloride, methanol according to the procedure described by Meyers and coworkers [57]. All the amino acid esters were characterized by spectral data, chiral high-performance liquid chromatography (HPLC) analysis, and by measuring specific rotation. The data matched well with the reported values [58–60]. The α_D values indicated that raceimization did not occur at this stage. Chiral HPLC analyses were carried out on a Daicel AD-H column (4.6× 250 mm) using acetonitrile (ACN) and isopropyl alcohol (IPA) as the eluent. In all the cases, 1.0 mg of the sample was dissolved in 1.0 mL of 1:1 CAN/IPA (95:5) mixture, out of which 2.0 μL was injected into HPLC having a flow rate 0.5 mL/min. Retention time at which the minor and the major enantiomer separated was calculated by maintaining the pressure max 14 kgf/cm^2 and at column temperature of 25 °C. The ee and de of the nitroketene N,S-acetals were computed from integration of peaks in the chiral HPLC chromatograms.

Representative procedure for the preparation of nitroketene N,S-acetals

N-Benzyl-N-[(E)-1-(methylsulfanyl)-2-nitro-1-ethenyl] amine-Lig_1 General procedure for nitroketene-N,S-acetal preparation as described by Poindexter and coworkers [58] was followed for the synthesis. However, acetonitrile was found to be better solvent for this conversion. Following the representative procedure described above, the reaction of 1,1-di(methylsulfanyl)-2-nitroethylene (5 g, 0.03 mol) with benzyl amine (3.2 g, 3.3 mL, 0.03 mol) in CH$_3$CN (25 mL) on 9 h reflux yielded N-benzyl-N-[(E)-1-(methylsulfanyl)-2-nitro-1-ethenyl]amine in 84 % (5.7 g) after recrystallization (20 % DCM-hexanes); mp 122 °C (EtOH); R_f 0.35 (8:2 hexane-EtOAc); IR (KBr) 3,136, 1,558, 1,462, and 1,347 cm^{-1}. ^{1}H-NMR (60 MHz, CDCl$_3$:CCl$_4$) δ 10.75 (br s, 1 H), 7.38–7.28 (m, 5 H), 6.58 (s, 1 H), 4.6 (d, J=5.9 Hz, 2 H), 2.4 (s, 3 H). MF: C$_{11}$H$_{14}$N$_2$O$_2$S; HRMS (ESI) calculated for [M+H]$^+$ 239.0854, found 239.0851.

N-[(E)-1-(methylsulfanyl)-2-nitro-1-ethenyl]-N-phenethyl-amine-Lig_2 Following the representative procedure described above, the reaction of 1,1-di(methylsulfanyl)-2-nitroethylene (5 g, 0.03 mol) with 2-phenyl-1-ethanamine (3.6 g, 3.8 mL, 0.03 mol) in CH$_3$CN (25 mL) on 3.5 h reflux yielded N-[(E)-1-(methylsulfanyl)-2-nitro-1-ethenyl]-N-phenethylamine in 72 % (5.2 g) after column purification with increasing amounts of EtOAc (5–20 %) in hexanes as eluent; mp 96–98 °C (EtOH); R_f 0.5 (8:2 hexane-EtOAc); UV (MeOH) λ_{max} 356 nm (logε=4.1), 271 nm (logε=3.4); IR (KBr) 3,142, 1,561, 1,462, 1,336 cm^{-1}; ^{1}H-NMR (60 MHz, CDCl$_3$:CCl$_4$, 1:1) δ 10.44 (br s, J=6.6 Hz, 1 H), 7.26 (s, 5 H), 6.47 (s, 1 H), 3.67 (t, J=7.2 Hz, 2 H), 3.03 (t, J=7.2 Hz, 3 H), 2.42 (s, 3 H); MF: C$_{10}$H$_{12}$N$_2$O$_2$S HRMS (ESI) calculated for [M+H]$^+$ 225.0698, found 225.0695.

N-[(E)-1-(methylsulfanyl)-2-nitro-1-ethenyl]-N-[(1S)-1-phenylethyl]amine-Lig_3 Following the representative procedure described above, the reaction of 1,1-di(methylsulfanyl)-2-nitroethylene (0.5 g, 0.003 mol) with 1-phenyl-1-ethanamine (0.37 g, 0.003 mol) in CH$_3$CN (12 mL) on 5 h reflux yielded N-[(E)-1-(methylsulfanyl)-2-nitro-1-ethenyl]-N-[(1S)-1-phenylethyl]amine in 50 % (0.36 g) after column purification using increasing amounts of EtOAc (10–20 %) in hexanes as eluent;

R_f 0.5 (7:3 hexane-EtOAc); UV (MeOH) λ_{max} 356 nm (logε= 4.9), 267 nm (logε=4.2), 223 nm (logε=4.8); IR (KBr) 3,159, 2,924, 1,556, 1,460, 1,370 cm^{-1}; ^{1}H-NMR (300 MHz, CDCl$_3$) δ 10.89 (br s, 1 H), 7.4–7.2 (m, 5 H), 6.56 (s, 1 H), 4.9 (pentet, J=7.2 Hz, 1 H), 2.37 (s, 3 H), 1.63 (d, J=7.2 Hz, 3 H);^{13}C-NMR (75 MHz, CDCl$_3$) δ 164.0 (C), 141.6 (C), 129.0 (2 × CH), 127.9 (CH), 125.8 (2×CH), 106.5 (CH), 54.7 (CH), 24.0 (Me), 14.5 (SMe); $[\alpha]_D^{25}$=+80 (C 0.08, MeOH, 44 % ee). HPLC: solvent ACN: IPA, 95:5; flow rate: 0.5 mL min^{-1}; retention times: 6.4 min (minor enantiomer) and 7.0 min (major enantiomer). MF: C$_{11}$H$_{14}$N$_2$O$_2$S HRMS (ESI) calculated for [M+H]$^+$ 239.0854, found 239.0851.

Representative procedure for the preparation of amino acid containing nitroketene N,S-acetals

Preparation of methyl (2S)-2-[(E)-1-(methylsulfanyl)-2-nitro-1-ethenyl]amino-3-phenylpropanoate-Lig_4 Following the representative procedure the reaction of 1,1-di(methylsulfanyl)-2-nitro-1-ethene (0.5 g, 3.0 mmol) with methyl (2S)-2-amino-3-phenylpropanoate (methyl phenylalaninate, 0.98 g, 4.5 mmol) in CH$_3$CN (15 mL) solvent on 24 h reflux provided 0. 51 g of methyl (2S)-2-[(E)-1-(methylsulfanyl)-2-nitro-1-ethenyl]amino-3-phenylpropanoate in 57 % yield as yellow solid after column purification using increasing amounts of EtOAc (10 % to 30 %) in hexanes; mp 108–110 °C (EtOH); R_f 0.5 (7:3 hexane-EtOAc); UV (MeOH) λ_{max} 356 nm (log ε= 5.0), 269 nm (logε=4.4), 214 nm (logε=4.8); IR (KBr) 3,159, 1,744, 1,559, 1,412, 1,325 cm^{-1}; ^{1}H-NMR (300 MHz, CDCl$_3$) δ 10.56 (br s, 1 H), 7.3–7.17 (m, 5 H), 6.51 (s, 1 H), 4.67 (dd, J=6.3, 5.1 Hz, 1 H), 3.76 (s, 3 H), 3.27 (dd, J=13.8 Hz, 5.1 Hz, 1 H), 3.16 (dd, J=13.8 Hz, 7.2 Hz, 1 H), 2.37 (s, 3 H); ^{13}C-NMR (75 MHz, CDCl$_3$) δ 169.9 (C), 163.2 (C), 134.6 (C), 129.2 (2×CH), 128.9 (2×CH), 127.7 (CH), 107.7 (C), 58.5 (CH), 52.9 (OMe), 39.0 (CH$_2$), 14.7 (SMe); $[\alpha]_D^{25}$= −46.0 (C 0.04, MeOH, 10 % ee). HPLC: solvent ACN: IPA, 95:5; flow rate: 0.5 mL min^{-1}; retention times: 6.5 and 6.6 min. MF: C$_{13}$H$_{16}$N$_2$O$_4$S HRMS (ESI) calculated for [M+H]$^+$ 297.0909, found 297.0903.

Preparation of methyl (2S,3S)-3-methyl-2-[(E)-1-(methylsulfanyl)-2-nitro-1-ethenyl]aminopentanoate-Lig_5 Following the representative procedure described above, the reaction of 1,1-di(methylsulfanyl)-2-nitro-1-ethene (0.5 g, 3.0 mmol) with methyl (2S,3S)-2-amino-3-methylpentanoate (methyl isoleucinate, 0.83 g, 4.5 mmol) in CH$_3$CN (15 mL) solvent on 18 h reflux, provided methyl (2S,3S)-3-methyl-2-[(E)-1-(methylsulfanyl)-2-nitro-1-ethenyl]aminopentanoate as light yellow solid after column purification with increasing amounts of EtOAc (10–20 %) in hexanes as eluent. Further purification by recrystallization provided methyl (2S,3S)-3-methyl-2-[1-(methylsulfanyl)-2-nitro-1-ethenyl]aminopentanoate in 53 % yield (0.42 g); mp 68–70 °C (EtOH); R_f 0.5 (6:4 hexane-

EtOAc); UV (MeOH) λ_{max} 355 nm (logε=4.5), 276 nm (logε=3.8); IR (KBr) 3,154, 2,965, 1,742, 1,556, 1,415 cm^{-1}; ^{1}H-NMR (60 MHz, CDCl$_3$:CCl$_4$) δ 10.4 (d, J=7.8 Hz, 1 H), 6.42 (s, 1 H), 4.28 (quartet, J=4.8 Hz, 1 H), 3.76 (s, 3 H), 2.46 (s, 3 H), 2.16 (m, 1 H), 1.45 (pentet, 2 H), 1.26–0.94 (m, 6 H); ^{13}C-NMR (100 MHz, CDCl$_3$) δ 169.9 (C), 163.5 (C), 107.4 (CH), 61.68 (CH), 52.6 (OMe), 38.4 (CH), 25.1 (CH$_2$), 15.5 (CH$_3$), 14.6 (SMe), 11.4 (CH$_3$); $[\alpha]_D^{25}$=+92.5 (C 0.06, MeOH, 89 % de). HPLC: solvent ACN: IPA, 95:5; flow rate: 0.5 mL min^{-1}; retention times: 6.9 min (minor enantiomer) and 6.6 min (major enantiomer). MF: C$_{10}$H$_{18}$N$_2$O$_4$S HRMS (ESI) calculated for [M+H]$^+$ 263.1066, found 263.1062.

Preparation of methyl (2S)-3-(1H-3-indolyl)-2-[(E)-1-(methylsulfanyl)-2-nitro-1-ethenyl]aminopropanoate-Lig_6 Following the representative procedure described above, the reaction of 1,1-di(methylsulfanyl)-2-nitro-1-ethene (0.5 g, 3.0 mmol) with methyl (2S)-2-amino-3-(1H-3-indolyl)propanoate (methyl tryptophanate, 1.15 g, 4.5 mmol) in CH$_3$CN (15 mL) solvent on 17 h reflux furnished 0.53 g of methyl (2S)-3-(1H-3-indolyl)-2-[(E)-1-(methylsulfanyl)-2-nitro-1-ethenyl]aminopropanoate in 48 % yield as yellow solid after column purification with increasing amounts of EtOAc (20–50 %) in hexanes; mp 82 °C (EtOH); R_f 0.5 (6:4 hexane-EtOAc); UV (MeOH) λ_{max} 326 nm (logε=4.1), 251 nm (logε=3.8); IR (KBr) 3,579, 3,346, 2,953, 1,740, 1,556 cm^{-1}; ^{1}H-NMR (60 MHz, CDCl$_3$:CCl$_4$) δ 10.6 (d, J= 7.8 Hz, 1 H), 8.6 (s, 1 H), 7.6–7.1 (m, 4 H), 6.5 (s, 1 H), 4.8–4.5 (m, 1 H), 3.68 (s, 3 H), 3.4 (d, J=6.0 Hz, 2 H), 2.28 (s, 3 H); ^{13}C-NMR (100 MHz, CDCl$_3$) δ 170.4 (C), 163.8 (C), 136.3 (C), 126.8 (C), 124.0 (CH), 122.2 (CH), 119.5 (CH), 118.0 (CH), 111.6 (CH), 108.0 (C), 107.4 (C), 57.4 (CH), 52.8 (OMe), 28.8 (CH$_2$); $[\alpha]_D^{25}$=−286.7 (C 0.08, MeOH, 73.0 % ee). HPLC: solvent ACN: IPA, 97.5:2.5; flow rate: 0.5 mL min^{-1}; retention times: 7.7 min (major enantiomer) and 8.4 min (minor enantiomer). MF: C$_{15}$H$_{17}$N$_3$O$_4$S HRMS (ESI) calculated for [M+H]$^+$ 336.1018, found 336.1015.

References

1. Atack JR, Perry EK, Bonham JR, Perry RH, Tomlinson BE, Blessed G, Fairbairn A (1983) Molecular forms of acetylcholinesterase in senile dementia of Alzheimer type: selective loss of the intermediate (10S) form. Neurosci Lett 40(2):199–204

2. Davies P, Maloney AJ (1976) Selective loss of central cholinergic neurons in Alzheimer's disease. Lancet 2(8000):1403

3. DeKosky ST, Scheff SW (1990) Synapse loss in frontal cortex biopsies in Alzheimer's disease: correlation with cognitive severity. Ann Neurol 27(5):457–464

4. Fishman EB, Siek GC, MacCallum RD, Bird ED, Volicer L, Marquis JK (1986) Distribution of the molecular forms of acetylcholinesterase in human brain: alterations in dementia of the Alzheimer type. Ann Neurol 19(3):246–252

5. Perry EK, Gibson PH, Blessed G, Perry RH, Tomlinson BE (1977) Neurotransmitter enzyme abnormalities in senile dementia. Choline acetyltransferase and glutamic acid decarboxylase activities in necropsy brain tissue. J Neurol Sci 34(2):247–265

6. Pfeffer RI, Afifi AA, Chance JM (1987) Prevalence of Alzheimer's disease in a retirement community. Am J Epidemiol 125(3):420–436

7. McGleenon BM, Dynan KB, Passmore AP (1999) Acetylcholinesterase inhibitors in Alzheimer's disease. Br J Clin Pharmacol 48(4):471–480

8. Kryger G, Silman I, Sussman JL (1999) Structure of acetylcholinesterase complexed with E2020 (Aricept): implications for the design of new anti-Alzheimer drugs. Structure 7(3):297–307

9. Harel M, Schalk I, Ehret-Sabatier L, Bouet F, Goeldner M, Hirth C, Axelsen PH, Silman I, Sussman JL (1993) Quaternary ligand binding to aromatic residues in the active-site gorge of acetylcholinesterase. Proc Natl Acad Sci U S A 90(19):9031–9035

10. Bar-On P, Millard CB, Harel M, Dvir H, Enz A, Sussman JL, Silman I (2002) Kinetic and structural studies on the interaction of cholinesterases with the anti-Alzheimer drug rivastigmine. Biochemistry 41(11):3555–3564

11. Rachinsky TL, Camp S, Li Y, Ekstrom TJ, Newton M, Taylor P (1990) Molecular cloning of mouse acetylcholinesterase: tissue distribution of alternatively spliced mRNA species. Neuron 5(3):317–327

12. Bourne Y, Taylor P, Marchot P (1995) Acetylcholinesterase inhibition by fasciculin: crystal structure of the complex. Cell 83(3):503–512

13. Sussman JL, Harel M, Frolow F, Oefner C, Goldman A, Toker L, Silman I (1991) Atomic structure of acetylcholinesterase from *Torpedo californica*: a prototypic acetylcholine-binding protein. Science 253(5022):872–879

14. Froede HC, Wilson IB (1984) Direct determination of acetyl-enzyme intermediate in the acetylcholinesterase-catalyzed hydrolysis of acetylcholine and acetylthiocholine. J Biol Chem 259(17):11010–11013

15. Mooser G, Sigman DS (1974) Ligand binding properties of acetylcholinesterase determined with fluorescent probes. Biochemistry 13(11):2299–2307

16. Taylor P, Lappi S (1975) Interaction of fluorescence probes with acetylcholinesterase. The site and specificity of propidium binding Biochemistry 14(9):1989–1997

17. Bourne Y, Radic Z, Sulzenbacher G, Kim E, Taylor P, Marchot P (2006) Substrate and product trafficking through the active center gorge of acetylcholinesterase analyzed by crystallography and equilibrium binding. J Biol Chem 281(39):29256–29267

18. Colletier J-P, Fournier D, Greenblatt HM, Stojan J, Sussman JL, Zaccai G, Silman I, Weik M (2006) Structural insights into substrate traffic and inhibition in acetylcholinesterase. EMBO J 25(12):2746–2756

19. Harel M, Quinn DM, Nair HK, Silman I, Sussman JL (1996) The X-ray structure of a transition state analog complex reveals the molecular origins of the catalytic power and substrate specificity of acetylcholinesterase. J Am Chem Soc 118(10):2340–2346

20. Belleau B, DiTullio V, Tsai YH (1970) Kinetic effects of leptocurares and pachycurares on the methanesulfonylation of acetylcholinesterase. A correlation with pharmacodynamic properties. Mol Pharmacol 6(1):41–45

21. Roufogalis BD, Quist EE (1972) Relative binding sites of pharmacologically active ligands on bovine erythrocyte acetylcholinesterase. Mol Pharmacol 8(1):41–49

22. Johnson JL, Cusack B, Davies MP, Fauq A, Rosenberry TL (2003) Unmasking tandem site interaction in human acetylcholinesterase. Substrate activation with a cationic acetanilide substrate. Biochemistry 42(18):5438–5452

23. Morel N, Bon S, Greenblatt HM, Van Belle D, Wodak SJ, Sussman JL, Massoulie J, Silman I (1999) Effect of mutations within the peripheral anionic site on the stability of acetylcholinesterase. Mol Pharmacol 55(6):982–992

24. Szegletes T, Mallender WD, Rosenberry TL (1998) Nonequilibrium analysis alters the mechanistic interpretation of inhibition of acetylcholinesterase by peripheral site ligands. Biochemistry 37(12):4206–4216

25. Szegletes T, Mallender WD, Thomas PJ, Rosenberry TL (1999) Substrate binding to the peripheral site of acetylcholinesterase initiates enzymatic catalysis. Substrate inhibition arises as a secondary effect. Biochemistry 38(1):122–133

26. Alvarez A, Bronfman F, Perez CA, Vicente M, Garrido J, Inestrosa NC (1995) Acetylcholinesterase, a senile plaque component, affects the fibrillogenesis of amyloid-beta-peptides. Neurosci Lett 201(1):49–52

27. Alvarez A, Opazo C, Alarcon R, Garrido J, Inestrosa NC (1997) Acetylcholinesterase promotes the aggregation of amyloid-beta-peptide fragments by forming a complex with the growing fibrils. J Mol Biol 272(3):348–361

28. Inestrosa NC, Alvarez A, Perez CA, Moreno RD, Vicente M, Linker C, Casanueva OI, Soto C, Garrido J (1996) Acetylcholinesterase accelerates assembly of amyloid-beta-peptides into Alzheimer's fibrils: possible role of the peripheral site of the enzyme. Neuron 16(4):881–891

29. Bartolini M, Bertucci C, Cavrini V, Andrisano V (2003) Beta-amyloid aggregation induced by human acetylcholinesterase: inhibition studies. Biochem Pharmacol 65(3):407–416

30. Barak D, Kronman C, Ordentlich A, Ariel N, Bromberg A, Marcus D, Lazar A, Velan B, Shafferman A (1994) Acetylcholinesterase peripheral anionic site degeneracy conferred by amino acid arrays sharing a common core. J Biol Chem 269(9):6296–6305

31. Radic Z, Pickering NA, Vellom DC, Camp S, Taylor P (1993) Three distinct domains in the cholinesterase molecule confer selectivity for acetyl- and butyrylcholinesterase inhibitors. Biochemistry 32(45):12074–12084

32. Farlow M, Gracon SI, Hershey LA, Lewis KW, Sadowsky CH, Dolan-Ureno J et al (1992) A controlled trial of Tacrine in Alzheimer's disease. JAMA: The Journal of the American Medical Association 268(18):2523–2529

33. Inglis F (2002) The tolerability and safety of cholinesterase inhibitors in the treatment of dementia. Int J Clin Pract Suppl 127:45–63

34. Watkins PB, Zimmerman HJ, Knapp MJ, Gracon SI, Lewis KW (1994) Hepatotoxic effects of tacrine administration in patients with Alzheimer's disease. JAMA 271(13):992–998

35. Winblad B, Grossberg G, Frolich L, Farlow M, Zechner S, Nagel J, Lane R (2007) IDEAL. Neurology 69(4):S14–S22, suppl 1

36. Galli A, Mori F, Benini L, Cacciarelli N (1994) Acetylcholinesterase protection and the anti-diisopropylfluorophosphate efficacy of E2020. Eur J Pharmacol 270(2–3):189–193

37. Rogers SL, Farlow MR, Doody RS, Mohs R, Friedhoff LT, Donepezil Study G (1998) A 24-week, double-blind, placebo-controlled trial of donepezil in patients with Alzheimer's disease. Neurology 50(1):136–145

38. Rogers SL, Friedhoff LT (1996) The efficacy and safety of Done-pezil in patients with Alzheimer's disease: results of a US multi-centre, randomized, double-blind, placebo-controlled trial. Dement Geriatr Cogn Disord 7(6):293–303

39. Daly MJ, Price BJ, Ellis GP, West GB (1983) 6 Ranitidine and other H2-receptor antagonists: Recent developments. Progress in Medicinal Chemistry 20:337–368

40. Yeomans ND, Svedberg LE, Naesdal J (2006) Is ranitidine therapy sufficient for healing peptic ulcers associated with non-steroidal anti-inflammatory drug use? Int J Clin Pract 60 (11):1401–1407

41. Gao Z, Li H, Zhang H, Liu X, Kang L, Luo X, Zhu W, Chen K, Wang X, Jiang H (2008) PDTD: a web-accessible protein database for drug target identification. BMC Bioinforma 9:104

42. Li H, Gao Z, Kang L, Zhang H, Yang K, Yu K, Luo X, Zhu W, Chen K, Shen J, Wang X, Jiang H (2006) TarFisDock: a web server for identifying drug targets with docking approach. Nucleic Acids Res 34:W219–W224, Web server issue

43. Anzali S, Barnickel G, Cezanne B, Krug M, Filimonov D, Poroikov V (2001) Discriminating between drugs and nondrugs by prediction of activity spectra for substances (PASS). J Med Chem 44(15):2432–2437

44. Lagunin A, Stepanchikova A, Filimonov D, Poroikov V (2000) PASS: prediction of activity spectra for biologically active substances. Bioinformatics 16(8):747–748

45. Jones G, Willett P, Glen RC (1995) Molecular recognition of receptor sites using a genetic algorithm with a description of desolvation. J Mol Biol 245(1):43–53

46. Jones G, Willett P, Glen RC, Leach AR, Taylor R (1997) Development and validation of a genetic algorithm for flexible docking. J Mol Biol 267(3):727–748

47. Kryger G, Harel M, Giles K, Toker L, Velan B, Lazar A, Kronman C, Barak D, Ariel N, Shafferman A, Silman I, Sussman JL (2000) Structures of recombinant native and E202Q mutant human acetylcholinesterase complexed with the snake-venom toxin fasciculin-II. Acta Crystallogr D: Biol Crystallogr 56(Pt 11):1385–1394

48. Bas DC, Rogers DM, Jensen JH (2008) Very fast prediction and rationalization of pKa values for protein–ligand complexes. Proteins 73(3):765–783

49. Zhang S, Iwata K, Lachenmann MJ, Peng JW, Li S, Stimson ER, Ya L, Felix AM, Maggio JE, Lee JP (2000) The Alzheimer's peptide A[beta] adopts a collapsed coil structure in water. J Struct Biol 130(2–3):130–141

50. Dominguez C, Boelens R, Bonvin AM (2003) HADDOCK: a protein–protein docking approach based on biochemical or bio-physical information. J Am Chem Soc 125(7):1731–1737

51. Rao HSP, Sakthikumar L, Vanitha S, Kumar SS (2003) Nitroketene dithioacetal chemistry. Part 2: synthesis of novel 4-(alkylsulfanyl)-2-[1-nitromethylidene]-1,3-dithioles from the dipotassium salt of 2-nitro-1,1-ethylenedithiol. Tetrahedron Letters 44(25):4701–4704

52. Rao SP, Sakthikumar L, Shreedevi S (2002) Nitroketene dithioacetal chemistry: synthesis and characterization of some 1,1-di (alkylsulfanyl)-2-nitroethylenes and 2-(nitromethylene)-1,3-dithia heterocycles. Sulfur Letters 25(5):207–218

53. Ertl P, Rohde B, Selzer P (2000) Fast calculation of molecular polar surface area as a sum of fragment-based contributions and its application to the prediction of drug transport properties. J Med Chem 43(20):3714–3717

54. Bartling A, Thiermann H, Szinicz L, Worek F (2005) Effect of metoclopramide and ranitidine on the inhibition of human AChE by VX in vitro. J Appl Toxicol 25(6):568–571

55. Solomon GC, Herrmann C, Vura-Weis J, Wasielewski MR, Ratner MA (2010) The chameleonic nature of electron transport through pi-stacked systems. J Am Chem Soc 132(23):7887–7889

56. Ordentlich A, Barak D, Kronman C, Ariel N, Segall Y, Velan B, Shafferman A (1998) Functional characteristics of the oxyanion hole in human acetylcholinesterase. J Biol Chem 273(31):19509–19517

57. Meyers AI, Williams DR, Erickson GW, White S, Druelinger M (1981) Enantioselective alkylation of ketones via chiral, nonrace-mic lithioenamines. An asymmetric synthesis of α-alkyl and α, α′-dialkyl cyclic ketones. J Am Chem Soc 103(11):3081–3087

58. Poindexter GS, Bruce MA, Breitenbucher JG, Higgins MA, Sit SY, Romine JL, Martin SW, Ward SA, McGovern RT, Clarke W, Russell J, Antal-Zimanyi I (2004) Dihydropyridine neuropeptide Y Y1 receptor antagonists 2: bioisosteric urea replacements. Bioorg Med Chem 12(2):507–521

59. Omata K, Aoyagi S, Kabuto K (2004) Observing the enantiomeric 1 H chemical shift non-equivalence of several [alpha]-amino ester signals using tris[3-(trifluoromethylhydroxymethylene)-(+)-camphorato]samarium(III): a chiral lanthanide shift reagent that causes minimal line broadening. Tetrahedron-Asymmetry 15(15):2351–2356

60. Tandon VK, Yadav DB, Singh RV, Chaturvedi AK, Shukla PK (2005) Synthesis and biological evaluation of novel (L)-alpha-amino acid methyl ester, heteroalkyl, and aryl substituted 1,4-naphthoquinone derivatives as antifungal and antibacterial agents. Bioorg Med Chem Lett 15(23):5324–5328